

Supporting Information

Dendritic Arrays of the $[\text{Re}_6(\mu_3\text{-Se})_8]^{2+}$ Core-Containing Clusters: Exploratory Synthesis and Electrochemical Studies

Bryan K. Roland, Ware H. Flora, Hugh D. Selby, Neal R. Armstrong, and Zhiping Zheng*

Department of Chemistry, University of Arizona, Tucson, Arizona 85721

E-mail: zhiping@u.arizona.edu

EXPERIMENTAL SECTION

Preparation of Compounds. Cluster solvates $[\text{Re}_6(\mu_3\text{-Se})_8(\text{PEt}_3)_5(\text{CH}_3\text{CN})](\text{SbF}_6)_2$ (**1**) and $[\text{Re}_6(\mu_3\text{-Se})_8(\text{CH}_3\text{CN})_6](\text{SbF}_6)_2$ (**8**) were prepared according to published procedures.¹ Other reagents were of commercial origin and were used as received. NMR (^1H and ^{31}P) spectra were recorded on a Varian Unity 300 spectrometer in CD_2Cl_2 solutions. Chemical shifts of ^{31}P NMR spectra were referenced to 85% H_3PO_4 (0.00 ppm, with negative values meaning upfield). ^{77}Se NMR spectra were recorded on a Bruker 500 spectrometer in CD_3CN solutions. Chemical shifts of ^{77}Se spectra were referenced to diphenyldiselenide (460 ppm; relative to a 6% solution (v/v) of dimethylselenide at 0.00 ppm in CD_3CN). Elemental analysis (CHN) was performed by Desert Analytics Laboratory, Tucson, Arizona.

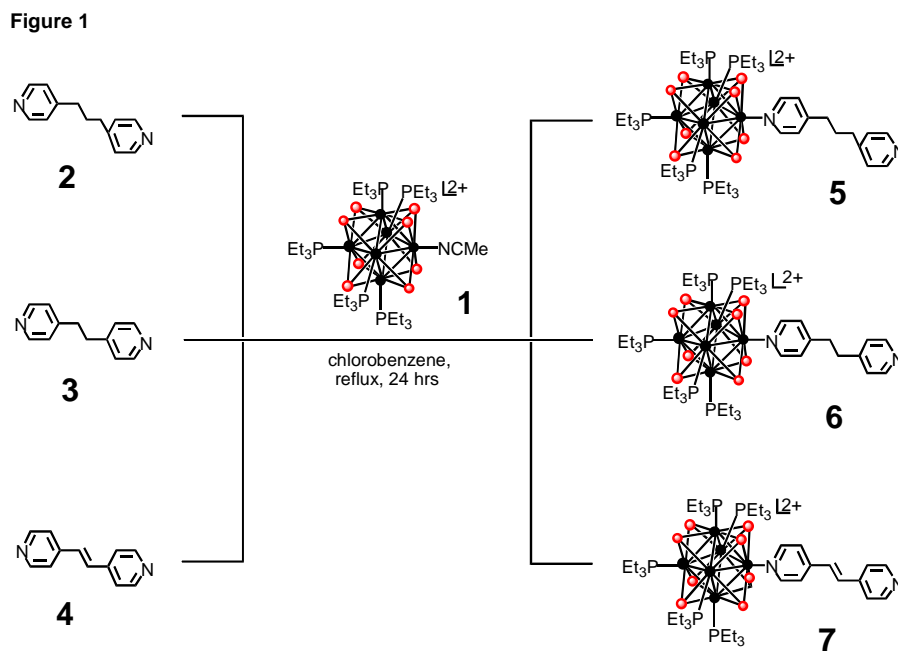


Figure 1. Synthesis of cluster complex ligands $[\text{Re}_6(\mu_3\text{-Se})_8(\text{PEt}_3)_5(\text{L})](\text{SbF}_6)_2$ [**5**, **6**, and **7**, wherein L = 4,4'-trimethylenedipyridine (**2**), 1,2-bis(4-pyridyl)ethane (**3**), and (*E*)-1,2-bis(4-pyridyl)ethene (**4**), respectively].

$[\text{Re}_6(\mu_3\text{-Se})_8(\text{PEt}_3)_5(\mathbf{2})](\text{SbF}_6)_2$ (5**).** A dichloromethane solution (10 mL) of $[\text{Re}_6(\mu_3\text{-Se})_8(\text{PEt}_3)_5(\text{CH}_3\text{CN})](\text{SbF}_6)_2$ (**1**, 0.259 g, 0.091 mmol) was added over 1 hour to a chlorobenzene solution (50 mL) of 4,4'-trimethylenedipyridine (**2**, 1.512 g, 7.63 mmol) under reflux. The reflux continued for an additional 24 hours. The solvent was removed *in vacuo* to give an orange-red oily residue, from which unreacted ligand **2** was removed by washing with toluene (4 x 50 mL). The resulting orange-red powder was flash chromatographed on a silica-gel column. The product was eluted with dichloromethane/acetonitrile (v/v, 5:1; $R_f = 0.50$), and was obtained as an orange-red solid (0.143 g, 52%) after removal of the solvent. ^1H NMR: δ 0.99-1.16 (m, 45), 2.05-2.30 (m, 30), 2.67-2.85(m, 6), 7.12 (d, 2), 7.21 (d, 2), 8.45 (d, 2), 9.12 (d, 2). ^{31}P NMR: δ -22.56 (4), -25.82 (1). ^{77}Se NMR: δ -306 (4), -361 (4). Anal. Calcd for $\text{C}_{43}\text{H}_{89}\text{N}_2\text{P}_5\text{Re}_6\text{Se}_8\text{Sb}_2\text{F}_{12}$: C, 17.16; H, 2.98; N, 0.93. Found: C, 17.05; H, 3.01; N, 0.95.

[Re₆(μ₃-Se)₈(PEt₃)₅(3)](SbF₆)₂ (6) was prepared in a manner analogous to the synthesis of **5**, starting with 1,2-bis(4-pyridyl)ethane (**3**, 0.860 g, 4.67 mmol) and [Re₆(μ₃-Se)₈(PEt₃)₅(CH₃CN)](SbF₆)₂ (**1**, 0.362 g, 0.127 mmol). The product was obtained as an orange-red powder (0.320 g, 85%). ¹H NMR: δ 1.00-1.40 (m, 45), 2.00-2.40 (m, 30), 3.10 (s, 4), 7.10 (d, 2), 7.42 (bs, 2), 8.55 (bs, 2), 9.10 (d, 2). ³¹P NMR: δ -21.67 (4), -24.97 (1). ⁷⁷Se NMR: δ -307 (4), -361 (4). Anal. Calcd for C₄₂H₈₇N₂P₅Re₆Se₈Sb₂F₁₂: C, 16.84; H, 2.93; N, 0.94. Found: C, 16.81; H, 2.96; N, 1.00.

[Re₆(μ₃-Se)₈(PEt₃)₅(4)](SbF₆)₂ (7) was prepared in a manner analogous to the synthesis of **5**, starting with (*E*)-1,2-bis(4-pyridyl)ethene (**4**, 0.901 g, 4.95 mmol) and [Re₆(μ₃-Se)₈(PEt₃)₅(CH₃CN)](SbF₆)₂ (**1**, 0.362 g, 0.127 mmol). The product was obtained as an orange-red powder (0.309 g, 82.7%). ¹H NMR: δ 1.00-1.60 (m, 45), 2.00-2.30 (m, 30), 7.35-7.53 (m, 6), 8.62 (d, 2), 9.20 (d, 2). ³¹P NMR: δ -24.95 (4), -28.29 (1). ⁷⁷Se NMR: δ -305 (4), -360 (4). Anal. Calcd for C₄₂H₈₅N₂P₅Re₆Se₈Sb₂F₁₂: C, 16.85; H, 2.86; N, 0.94. Found: C, 16.79; H, 2.93; N, 0.97.

{Re₆(μ₃-Se)₈[Re₆Se₈(PEt₃)₅(2)]₆}(SbF₆)₁₄ (9). A mixture of **5** (0.140 g, 0.0465 mmol) and the previously reported cluster solvate [Re₆(μ₃-Se)₈(CH₃CN)₆](SbF₆)₂ (**8**, 0.019 g, 0.0077 mmol) in 75 mL of chlorobenzene was brought to reflux under nitrogen. The reflux continued for 3 hours to produce an orange-red powder with a light-yellow supernatant. The solid was collected and re-dissolved in 2 mL of dichloromethane to yield an orange-red solution. Triturating this solution with diethyl ether afforded a light brown solid which was subsequently subjected to Soxhlet extraction with chlorobenzene for 48 hours. The product was obtained as an ochre-colored solid (0.070 g, 50%). ¹H NMR: δ 1.05-1.30 (m, 270), 2.15-2.35 (m, 180), 7.10-7.35 (md, 36), 9.15 (d, 12), 9.55 (d, 12). ³¹P NMR: δ -19.10 (24), -22.42 (6). ⁷⁷Se NMR: δ -248

(8), -307 (24), -360 (24). Anal. Calcd for $C_{258}H_{534}N_{12}P_{30}Re_{42}Se_{56}Sb_{14}F_{84}$: C, 15.28; H, 2.65; N, 0.83. Found: C, 15.30; H, 2.76; N, 0.82.

$\{Re_6(\mu_3-Se)_8[Re_6Se_8(PEt_3)_5(3)]_6\}(SbF_6)_{14}$ (**10**) was obtained analogously by reacting **8** (0.020 g, 0.0081 mmol) with **6** (0.100 g, 0.0333 mmol). After similar work-up and purification procedures, the product was obtained as an ochre-colored solid (0.080 g, 68%). 1H NMR: δ 1.05-1.40 (m, 270), 2.10-2.40 (m, 180), 3.10 (s, 24), 7.20-7.40 (md, 24), 9.15 (d, 12), 9.55 (d, 12). ^{31}P NMR: δ -24.89 (24), -28.56 (6). ^{77}Se NMR: δ -249 (8), -307 (24), -361 (24). Anal. Calcd for $C_{252}H_{522}N_{12}P_{30}Re_{42}Se_{56}Sb_{14}F_{84}$: C, 14.99; H, 2.61; N, 0.83. Found: C, 15.19; H, 2.66; N, 0.94.

$\{Re_6(\mu_3-Se)_8[Re_6Se_8(PEt_3)_5(4)]_6\}(SbF_6)_{14}$ (**11**) was obtained analogously by reacting **8** (0.020 g, 0.0081 mmol) with **7** (0.150 g, 0.0500 mmol) in 75 mL of chlorobenzene under reflux. After similar work-up and purification procedures, the product was obtained as an ochre-colored solid (0.080 g, 50%). 1H NMR: δ 1.05-1.20 (m, 270), 2.10-2.30 (m, 180), 7.40-7.60 (md, 36), 9.20 (d, 12), 9.65 (d, 12). ^{31}P NMR: δ -24.93 (24), -28.43 (6). ^{77}Se NMR: δ -240 (8), -305 (24), -360 (24). Anal. Calcd for $C_{252}H_{510}N_{12}P_{30}Re_{42}Se_{56}Sb_{14}F_{84}$: C, 15.00; H, 2.55; N, 0.83. Found: C, 15.33; H, 2.67; N, 1.02.

X-ray Structure Determinations. An orange block of **6** having approximate dimensions of 0.09 x 0.10 x 0.27 mm was mounted on a glass fiber in a random orientation. Examination of the crystal on a Bruker SMART 1000 CCD detector X-ray diffractometer at 170 K and a power setting of 50 KV, 40mA showed measurable diffraction to at least $\theta = 25.0^\circ$. Data were collected on the SMART1000 system using graphite monochromated Mo $K\alpha$ radiation ($\lambda = 0.71073 \text{ \AA}$). Cell constants and an initial orientation matrix were determined from reflections obtained in three orthogonal 5° wedges of reciprocal space. A total of 4898 frames at a detector

setting covering $0^\circ < 2\theta < 60^\circ$ were collected, having an omega scan width of 0.15° and an exposure time of 10 seconds. The frames were integrated using the Bruker SAINT software package's narrow frame algorithm. A total of 80327 reflections were integrated and retained, of which 16388 were unique, of which 12908 (78.8%) were observed $I > 2\sigma(I)$. The final monoclinic cell parameters of $a = 16.9603(10) \text{ \AA}$, $b = 20.6955(9) \text{ \AA}$, $c = 20.1896(10) \text{ \AA}$, $\alpha = 90^\circ$, $\beta = 96.263(2)^\circ$, $\gamma = 90^\circ$, volume = $7044.3(6) \text{ \AA}^3$ are based on the refinement of the XYZ-centroid of 986 reflections with $I > 20\sigma(I)$ covering the range of $2.2^\circ < \theta < 25.0^\circ$. Empirical absorption and decay corrections were applied using the program SADABS. The absorption coefficient is 15.330 mm^{-1} , $T_{\text{min}} = 0.1029$, and $T_{\text{max}} = 0.3557$. For $Z = 4$ and a formula weight of 2995.37, the calculated density is 2.824 g/cm^3 . Systematic absences and intensity statistics indicate the space group to be $P2(1)/n$, consistent with refinement.

The structure was solved using SHELXS in the Bruker SHELXTL (Version 5.0) software package. Refinements were performed using SHELXL and illustrations were made using XP. Solution was achieved utilizing direct methods followed by Fourier synthesis. Hydrogen atoms were added at idealized positions, constrained to ride on the atom to which they are bonded and given thermal parameters equal to 1.2 or 1.5 times U_{iso} of that bonded atom. The final anisotropic full-matrix least squares refinement based on F^2 of all reflections converged (maximum shift/esd = 0.005) at $R1 = 0.0417$, $wR2 = 0.0790$ and goodness-of-fit = 1.057. "Conventional" refinement indices using the 12908 reflections with $F > 4\sigma(F)$ are $R1 = 0.0299$, $wR2 = 0.0753$. The model consisted of 662 variable parameters, X constraints, and 13 restraints. There were 18 correlation coefficients between 0.694 and 0.5. All correlation coefficients were between the thermal parameters of the multiple fluorine atoms with unresolved disorder. The highest and lowest peaks on the final difference map were 2.190 and -2.170 e/mm^3 , respectively.

The structure of **6** is depicted in Figure 2. Crystallographic data and key inter atomic distances and angles are listed in Tables 1 and 2.

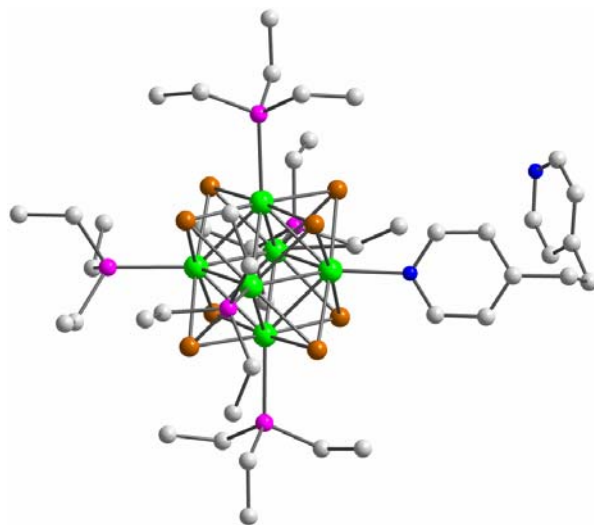


Figure 2. Crystal structure of the cationic cluster $[\text{Re}_6(\mu_3\text{-Se})_8(\text{PEt}_3)_5(\mathbf{3})]^{2+}$ (**6**). Color scheme: C (gray), N (blue), P (purple), Re (green), and Se (brown). The *gauche* conformation adopted by the non-phospine ligand **3** [1,2-bis(4-pyridyl)ethane] is clearly shown. Hydrogen atoms are omitted for clarity.

Table 1. Crystallographic Data and Structural Refinement of **6**.

Empirical formula	$C_{42}H_{87}F_{12}N_2P_5Re_6Sb_2Se_8$
Formula weight	2995.37
Crystal size	0.27 x 0.10 x 0.09 mm
Crystal system	Monoclinic
Space group	$P2_1/n$
Unit cell dimensions	$a = 16.960(10) \text{ \AA}$ $\beta = 96.263(2)^\circ$ $b = 20.695(9) \text{ \AA}$ $c = 20.184(10) \text{ \AA}$
Volume, Z	$7044.3(6) \text{ \AA}^3$, 4
Density, calcd Mg/m^3	2.824
Abs. coeff., mm^{-1}	15.330
$F(000)$	5440
Theta range for data collection	1.41 to 28.34°
Limiting indices	$-22 \leq h \leq 22$, $-27 \leq k \leq 27$, $-26 \leq l \leq 25$
Reflections utilized	80327
Independent reflections	16388 [R(int) = 0.0472]
Data/restraint/parameter	16388/13/662
GOF on F^2	1.057
R indices [$I > 2\sigma(I)$]	R1 = 0.0229, wR2 = 0.0753
R indices (all data)	R1 = 0.0417, wR2 = 0.0790

Table 2. Selected bond lengths (Å) and angles (°) of **6**.

Bond lengths	
Re-Re	2.629(1)-2.646(1); mean 2.636
Re-Se	2.505(6)-2.533(6); mean 2.517
Re-P	2.466(15)-2.479(4); mean 2.476
Re-N	2.203(4)
Bond angles	
Re-N-C	121.5(4) and 121.8(4)

Other Physical Measurements. Electronic absorption spectra in dichloromethane solutions were recorded on a Perkin Elmer Lambda 10 spectrophotometer. Cyclic voltammetry (CV) data were acquired with an EG & G Instruments 283 potentiostat, using a 500- μm diameter Pt working electrode, a freshly prepared Ag/AgCl reference electrode, and a Pt counter electrode. The working electrode was cleaned between each experiment by polishing with 0.3- μm alumina paste for 1 minute, followed by copious solvent rinses. The reference electrode was prepared by plating a thin layer of AgCl onto an Ag wire from a 1.0 M KCl solution. A custom glass solution cell with fritted openings was used to stabilize the electrodes and minimize permeation of oxygen. All measurements were carried out in nitrogen-degassed solutions containing tetrabutylammonium hexafluorophosphate as supporting electrolyte. Prior to preparing analyte solutions, the distilled solvent was run through a fresh column of activated alumina to remove trace water. Unless otherwise noted, an analyte concentration of *ca.* 1 mM, a scan rate (v) of 100 mV/s, and an electrolyte concentration of 0.1 M was used. After each voltammetric experiment, ferrocene was added (*ca.* 1 mM), an additional voltammogram was recorded, and the potential axis was calibrated against the formal potential for the ferrocenium/ferrocene (Fc^+/Fc) redox couple. Reported redox potentials represent the half-wave potential in these voltammograms.

In order to obtain coulometric information for the relevant redox event by performing exhaustive electrolysis on analyte solutions, a thin-layer electrochemical cell (TLE) was fabricated based on earlier designs from this group.² A schematic drawing of this cell is presented in Figure 3. The electrode was designed such that these measurements could be made using the above setup for standard CV, where the working electrode is simply replaced with an electrode shield. The entire electrode assembly was placed in the solution cell, and the distal end was submerged 2-5 mm into the analyte solution, causing the solution to reproducibly fill the

entire cavity formed between the Pt wire and the small capillary due to capillary action. Relatively large electrolyte concentrations (0.3 M) were necessary to minimize the potential drop in the TLE cavity. Thin-layer cyclic voltammograms (TLCV) were collected at 1 mV/s where there was insignificant diffusion dependence on the current. The cell volume was calibrated using a 1.0 mM standard solution of ferrocene in acetonitrile. Following the confirmation of a one-electron oxidation for the free cluster monomer **1**, standard solutions of **1** were used for volume calibration prior to analyzing multicluster molecules. Solvent background (minimal) was subtracted from all charge measurements.

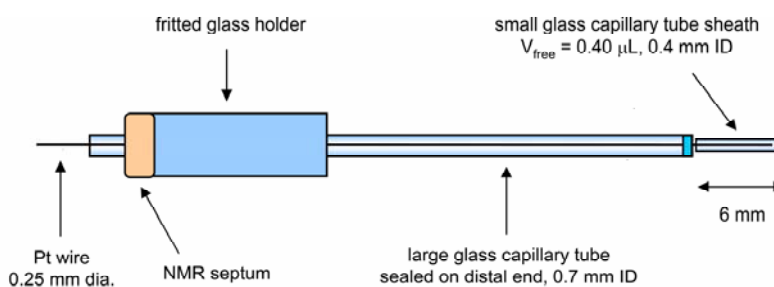


Figure 3. Schematic of thin-layer cell electrode.

Thin-layer cyclic voltammetry and advantages/disadvantages over standard voltammetry.

Coulometric measurements using a thin-layer cell electrode (TLE) are made possible by the confinement of the redox species provided by the thin layer. For such a case, at sufficiently slow scan rates (v , developed below), the current measured in a voltammetric experiment has no dependence on mass transfer in the cell, and it is therefore not necessary to know the diffusion coefficient (D_0) of the redox species in order to determine the number of electrons transferred per redox event (n).¹ While the peak current in such a voltammogram is directly proportional to v ,

the total amount of charge passed (Q) in exhaustively oxidizing/reducing the contents of such a thin layer is independent of v and can be related to n by the following formalism

$$Q = nFCV \quad (1)$$

where F is Faraday's constant, C is the bulk analyte concentration, and V is the cell volume.³ In addition to allowing for coulometric measurements to be made, this confinement of the redox species creates sharper peaks in the cyclic voltammetry, because at potentials substantially past the redox potential ($E^{\circ'}$) for the redox couple, all redox species in the cell are oxidized/reduced, and the current returns to the baseline. In standard voltammetry experiments this is not the case due to diffusion of bulk redox species to the electrode surface, where the current decays with time (t) at a rate of $t^{-1/2}$. Thin-layer voltammetry is additionally superior to standard voltammetry in that background charging current may be decreased without significantly decreasing the Faradaic (signal) current by utilizing slower sweep rates.

Despite these enhancements, there is a significant disadvantage associated with this technique: acquisition of voltammograms requires a substantially larger amount of time due to scan rates which must be much slower than for standard cyclic (100 mV/s) or differential pulse (20 mV/s) voltammetry. For Equation 1 to be valid for a thin-layer experiment, the scan time (t) must be significantly larger than the amount of time required to exhaustively oxidize/reduce the entire contents of the cell when the electrode is poised at a potential past $E^{\circ'}$ for the redox couple, which is described by the following equation¹

$$t \gg \frac{l^2}{2D_0} \quad (2)$$

For the thin-layer cell described above, with an l value of ca. 75 μm , and for a small organic molecule with a typical D_0 (10^{-5} cm^2/s), this translates to a t of 2.8 s which creates an equality

between the left and right hand sides of Equation 2. Scan time may be related to scan rate using the following equation

$$v = \frac{\Delta E}{t} \quad (3)$$

where ΔE is the difference between the initial and final potentials of the potential sweep through the redox event. A typical oxidation/reduction peak is ca. 500 mV wide under ideal thin-layer conditions with this TLE, giving a v of 178 mV/s which corresponds to an equality between the left and right hand sides of Equation 2. A scan rate of 18 mV/s or lower is advisable for this electrode/molecule combination in order to produce a voltammogram that is predominantly free of diffusion-limited current behavior and which facilitates accurate coulometric measurements. For large, dendrimer-like organic molecules (i.e. MW > 1500), with diffusion coefficients on the order of 10^{-6} cm²/s, analogous calculations translate into an advisable scan rate of 2 mV/s; for extremely large supramolecular materials such as those described in this chapter (i.e. MW > 10,000), with diffusion coefficients possibly as low as 10^{-7} cm²/s, scan rates of 0.2–1 mV/s are advisable.

These requirements dictate that a voltammogram for the materials studied here may take as long as 20 minutes to acquire, which is substantially longer than the 15 s required for a standard voltammogram of the same oxidation event. Despite the intentions of the most patient investigator, if the oxidized/reduced analyte is not stable on these extremely long time scales, reversible electrochemistry will not be obtained. This may be remedied to some extent, however, by designing the electrode with a smaller gap distance, allowing for faster scan rates. It is fortunate for the sake of the studies described here, however, that the single oxidation products for the $[\text{Re}_6(\mu_3\text{-Se})_8]^{2+}$ metal clusters are impressively stable on these time scales. TLCVs for the materials described here were accordingly collected at 1 mV/s or 0.5 mV/s.

Electrode qualification/characterization. Proper function of the TLE was verified in performing TLCV experiments on a 1 mM standard solution of ferrocene (Fc) in acetonitrile, a representative TLCV (10 mV/s) of which is presented in Figure 4. The shape of the Fc TLCV suggests that the TLE performs properly, where the current has no dependence on rates of diffusion (i.e. current returns to zero after exhaustively oxidizing the cell contents). In a theoretically ideal TLCV, the potential separation between the cathodic and anodic peaks (ΔE_p) is 0 mV, but it is typically ca. 40-100 mV here due to the potential gradient created inside the TLE cavity. Smaller ΔE_p values may be obtained at decreased scan rates and increased electrolyte concentrations, however, the modest ΔE_p values here bear no significance on the coulometric measurement.

The TLE volume was initially calibrated from these Fc voltammograms. The overall charge passed (Q) was measured by integrating the area underneath the anodic sweep of the oxidation of Fc to the Fc^+ ion (a well known one electron process) and dividing by the scan rate (45.0 μC). V was then calculated from Equation 1, yielding cell volumes (0.466 μL) comparable to the theoretical volume based on geometrical arguments. Uncertainties in the filled volume of the TLE cavity were consistently on the order of 0.01 μL (2% rel. std. dev. for $n = 3$) for such electrodes, yielding nearly identical voltammograms upon repeated filling/analysis. Following the confirmation of a one-electron oxidation for $[\text{Re}_6(\mu_3\text{-Se})_8(\text{PEt}_3)_5(\text{MeCN})](\text{SbF}_6)_2$ (**1**) the free cluster monomer, standard solutions of **1** were used for volume calibration prior to analyzing multi-cluster molecules. Electrode volumes varied from experiment to experiment because the electrode was frequently cleaned and re-fabricated.

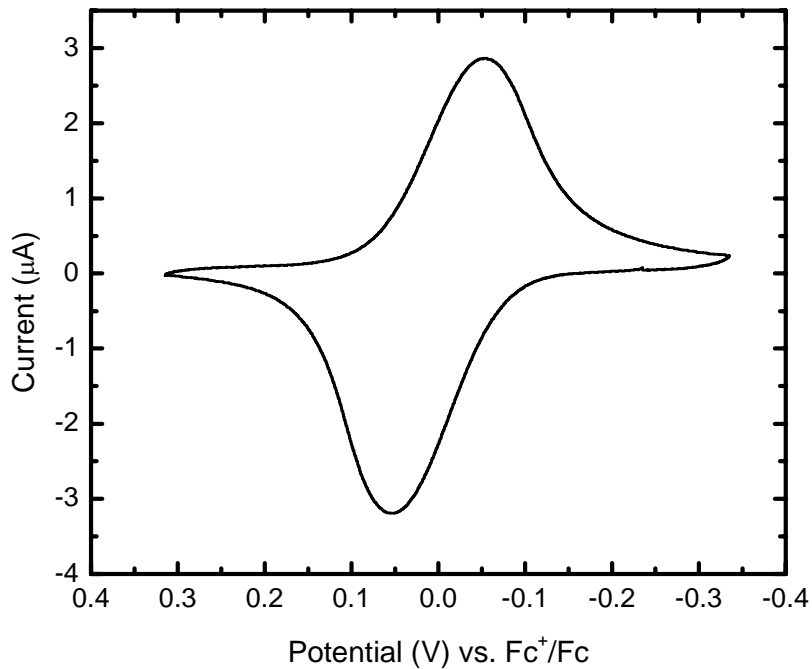


Figure 4: Thin-layer cyclic voltammogram for 1 mM ferrocene in acetonitrile. CVs such as this one were initially used to calibrate the volume of the TLE by integrating the anodic peak (45 μC). This specific TLE was determined to have a volume of 0.47 μL . Uncertainties in the filled volume of the TLE cavity were consistently on the order of 0.01 μL (2 % rel. std. dev. for $n = 3$) for such electrodes, yielding nearly identical voltammograms for repeated filling/analysis. Because of the small size (fast diffusion) of Fc, scan rates of 10 mV/s were sufficiently slow for the current response to be characteristic of exhaustive electrolysis (no diffusion dependence, current returns to zero). The peak separation (100 mV/s) is due to the potential gradient inside the TLE cavity and can be decreased to some extent with increasing electrolyte concentration.

Models for cluster dendrimer oxidation processes. The above voltammetric observations are discussed in further detail here in the context of hypothetical models which attempt to explain these results. A model describing the oxidative processes for **9** $\{\text{Re}_6(\mu_3\text{-Se})_8[\text{Re}_6(\mu_3\text{-Se})_8(\text{PEt}_3)_5(\text{L})]_6\}(\text{SbF}_6)_{14}$ (L=4,4'-trimethylenedipyridine) is presented in Figure 5, where the specific linker group (trimethylene) is implied by the black rectangle in the molecular structure. It is important to note that each $[\text{Re}_6(\mu_3\text{-Se})_8]^{2+}$ cluster has an inherent charge of 2+, giving all of the native cluster 7-mers an overall charge of 14+. In solution, electroneutrality must be maintained, and these charges are balanced with counter ions from the supporting electrolyte. In the case of the tetrabutylammonium hexafluorophosphate electrolyte used here, the positive charges on these clusters are balanced with PF_6^- anions (two for each cluster). At potentials below 0.5 V, as shown in Figure 5a, 14 anions are associated with the 7-mer. As the potential is increased to the $E^{\circ'}$ for the cluster oxidation (0.7 V, Figure 5b), all of the clusters on **9**, including the core cluster, are oxidized nearly simultaneously. In order to balance the additional 7+ charge incurred upon the removal of an electron from each cluster ($\text{Re}^{\text{III}} \rightarrow \text{Re}^{\text{IV}}$), 7 counter ions must diffuse into close contact with the clusters, despite their small separation distance. Based on the TLCV of this material, however, this process is not significantly hindered. Past the $E^{\circ'}$ for the cluster oxidation ($E > 0.9$ V, Figure 5c), this process is completed for all molecules in close proximity to the electrode surface, yielding a molecule with a 21+ charge and 21 associated counter ions.

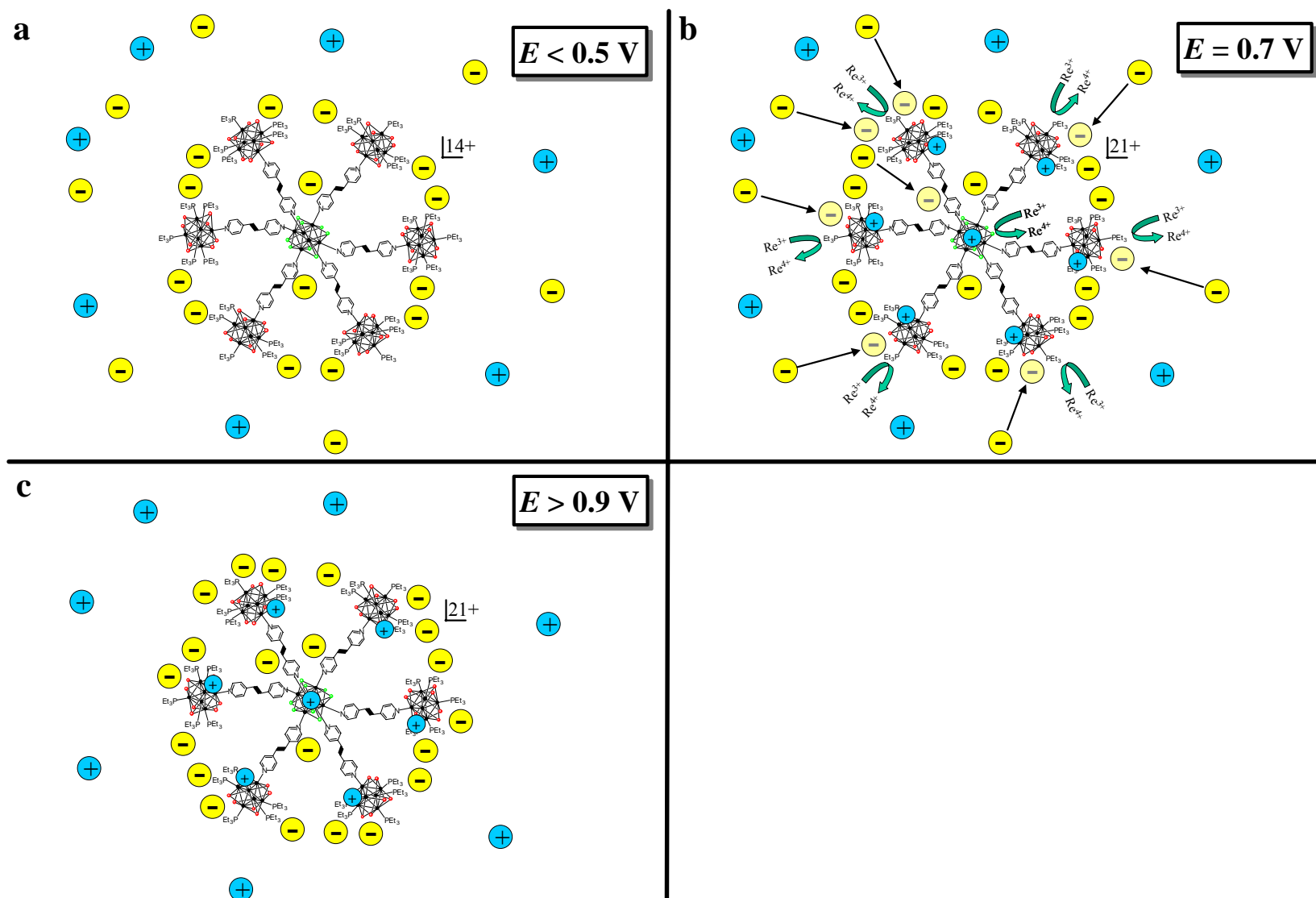


Figure 5: Model for **9** oxidation processes.

A model which describes the oxidation processes for **10** $\{\text{Re}_6(\mu_3\text{-Se})_8[\text{Re}_6(\mu_3\text{-Se})_8(\text{PEt}_3)_5(\text{L})]_6\}(\text{SbF}_6)_{14}$ [L=1,2-bis(4-pyridyl)ethane] is presented in Figure 6. The specific linker group (ethyl) is implied by the black rectangle in the molecular structure. The initial state of this molecule, at potentials below $E^{\circ'}$ (Figure 6a), is identical to **9**. As the potential is increased to $E^{\circ'}$ (0.7 V, Figure 6b), most of the clusters are immediately oxidized, and counter ions diffuse into close contact to balance the increased positive charge. Because of the decreased length of the linker group (one bond length), the clusters on this molecule are closer together than in **9**. This decreased spacing is substantial enough that diffusion of all 7 counter ions needed for the electroneutral oxidation of all clusters may be somewhat impeded and/or coulombic/steric screening of some clusters may take place. Either or both of these factors would contribute to the kinetically hindered oxidation of the final clusters on the molecule, which eventually are oxidized after enough time has passed (Figure 6c). As the potential is increased past $E^{\circ'}$ ($E > 0.9$ V, Figure 6d), this process is completed for all molecules in close proximity of the electrode surface and the cluster is fully oxidized.

Although the difference in one bond length of the linker may not immediately suggest sufficient cause for such a dramatic effect, it is important to consider that the charge density of the molecule (large values of which may impede further oxidation) is inversely proportional to the molecular volume, which for a sphere, is a function of r^3 . This difference in bond length was substantial enough to result in a more difficult synthesis of this material, over **9**, presumably due to increased coulombic and steric repulsion, in competition with the convergent synthesis.

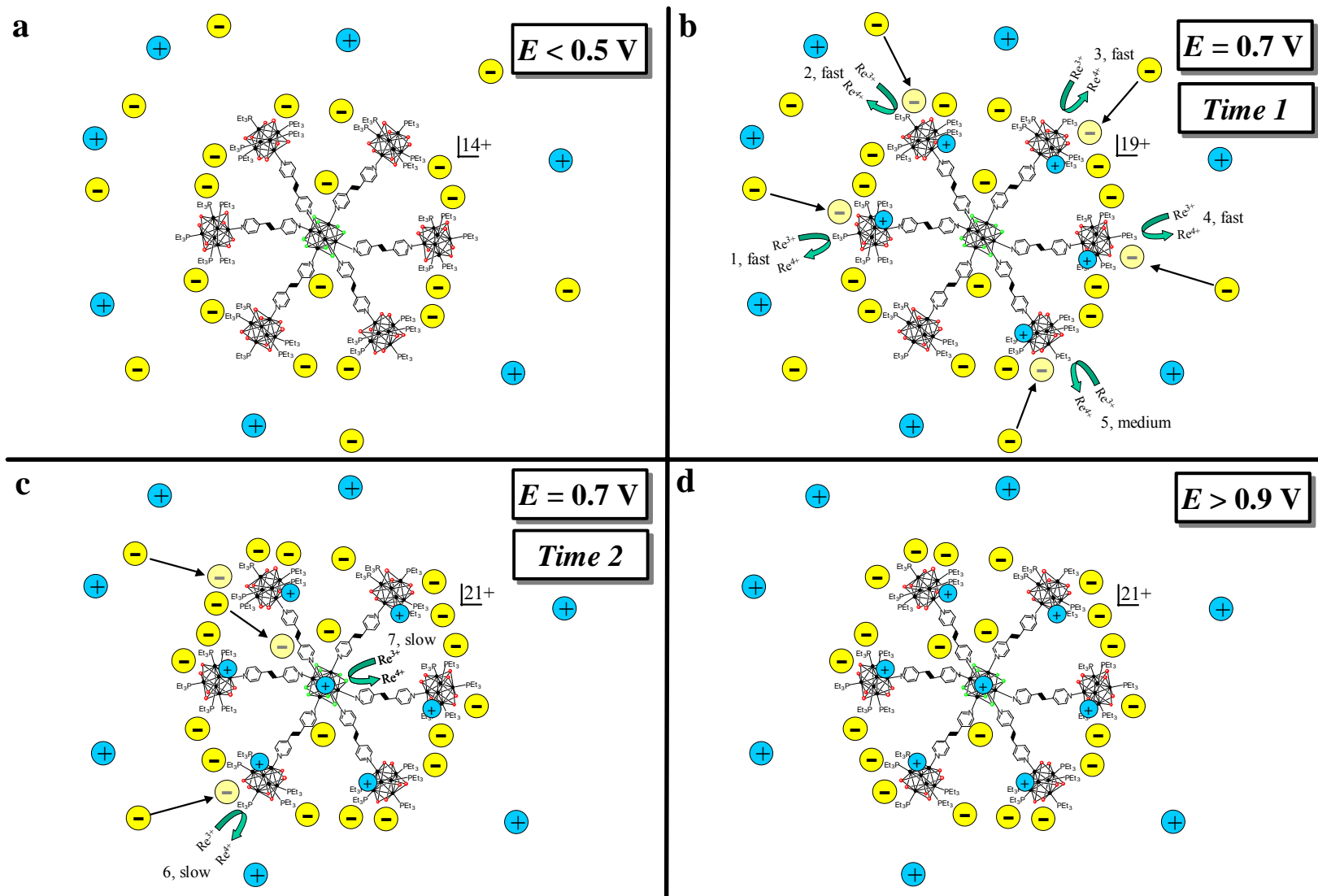


Figure 6: Model for 10 oxidation processes.

Additionally, efforts to create such molecular architectures as these cluster 7-mer dendrimers were not successful with linking bidentate ligands shorter than those used in **10**. With these considerations in mind, it is quite reasonable that such observations were noted and impressive that **9** was so readily oxidized to completion.

The oxidative processes of **11** $\{\text{Re}_6(\mu_3\text{-Se})_8[\text{Re}_6(\mu_3\text{-Se})_8(\text{PEt}_3)_5(\text{L})]_6\}(\text{SbF}_6)_{14}$ [L=(*E*)-1,2-bis(4-pyridyl)ethane] are modeled in Figure 7, where the linker group (ethene) is implied by the black rectangle in the molecular structure. The overall length of the bidentate linking ligand for this material is expected to be fairly comparable to the ligand length for **10** above. The initial state of the **11** molecule at potentials below $E^{\circ'}$ (Figure 7a) is comparable to the other materials. Once the potential approaches $E^{\circ'}$ (Figure 7b), the more accessible peripheral clusters begin to oxidize. Because of the complete conjugation of this linking ligand (which the previous two materials lack), the excess positive charge of this molecule is somewhat delocalized across the organic ligands. The creation of oxidized clusters, with a local charge of 3+, results in some through-bond polarization of the core cluster, imparting a partial positive charge which increases with each cluster oxidized on the periphery. Due to this electrical communication between the peripheral and core clusters, the core cluster becomes more difficult to oxidize and is not oxidized at the $E^{\circ'}$ for the oxidation of the peripheral clusters. As the potential is increased to the second $E^{\circ'}$ for the molecule (0.9 V, Figure 7c), the core cluster is oxidized, and by potentials greater than 0.9 V (Figure 7d), all molecules in proximity of the electrode surface are completely oxidized.

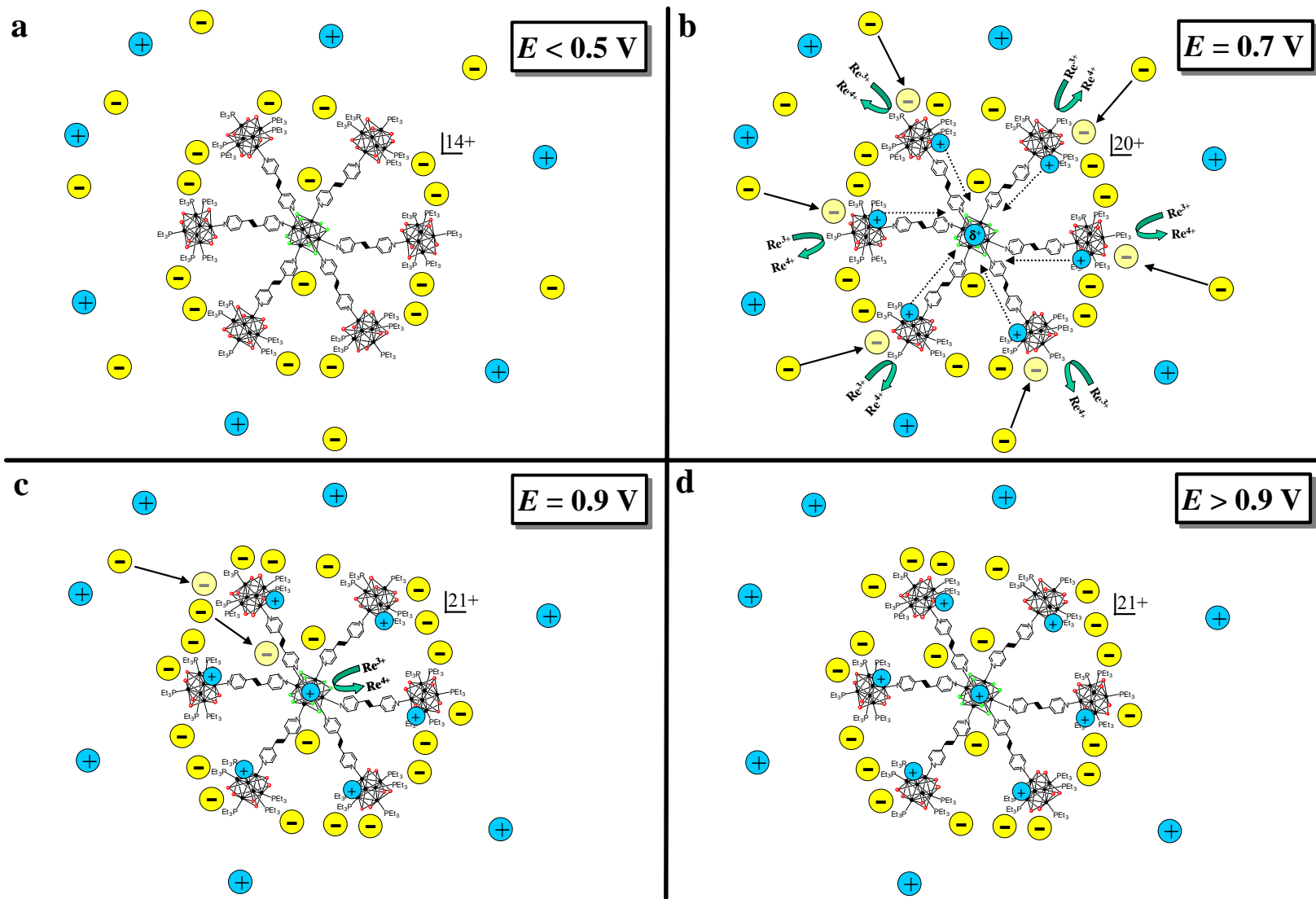


Figure 7: Model for 11 oxidation processes.

References

1. Zheng, Z.; Long, J. R.; Holm, R. H. *J. Am. Chem. Soc.* **1997**, *119*, 2163.
2. Flora, W.; Ph.D. Dissertation, University of Arizona, 2005.
3. Bard, A. J.; Faulkner, L. R. *Electrochemical Methods: Fundamentals and Applications*; 2 ed.; John Wiley & Sons: New York, 2001.